

## Site-testing at Muztagh-ata site I: ground meteorology and sky brightness

Jing Xu<sup>1,2</sup>, Ali Esamdin<sup>1,2</sup>, Jin-Xin Hao<sup>3</sup>, Jin-Min Bai<sup>4</sup>, Ji Yang<sup>5</sup>, Xu Zhou<sup>3</sup>, Yong-Qiang Yao<sup>3</sup>, Jin-Liang Hou<sup>6</sup>, Guang-Xin Pu<sup>1</sup>, Guo-Jie Feng<sup>1,2</sup>, Chun-Hai Bai<sup>1</sup>, Peng Wei<sup>1</sup>, Shu-Guo Ma<sup>1</sup>, Abudusaimaitijiang Yisikandee<sup>1</sup>, Le-Tian Wang<sup>1</sup>, Xuan Zhang<sup>1</sup>, Liang Ming<sup>1</sup>, Lu Ma<sup>1</sup>, Jin-Zhong Liu<sup>1</sup>, Zi-Huang Cao<sup>2,3</sup>, Yong-Heng Zhao<sup>3</sup>, Lu Feng<sup>3</sup>, Jian-Rong Shi<sup>3</sup>, Hua-Lin Chen<sup>7</sup>, Chong Pei<sup>7</sup>, Xiao-Jun Jiang<sup>3</sup>, Jian-Feng Wang<sup>3</sup>, Jian-Feng Tian<sup>3</sup>, Yan-Jie Xue<sup>3</sup>, Jing-Yao Hu<sup>3</sup> and Yun-Ying Jiang<sup>3</sup>

<sup>1</sup> Xinjiang Astronomical Observatory, Chinese Academy of Sciences, Urumqi 830011, China; [xujing@xao.ac.cn](mailto:xujing@xao.ac.cn); [aliyi@xao.ac.cn](mailto:aliyi@xao.ac.cn)

<sup>2</sup> University of Chinese Academy of Sciences, Beijing 100049, China

<sup>3</sup> National Astronomical Observatories, Chinese Academy of Sciences, Beijing 100101, China

<sup>4</sup> Yunnan Observatories, Chinese Academy of Sciences, Kunming 650000, China

<sup>5</sup> Purple Mountain Observatory, Chinese Academy of Sciences, Nanjing 210008, China

<sup>6</sup> Shanghai Astronomical Observatory, Chinese Academy of Sciences, Shanghai 200030, China

<sup>7</sup> Nanjing Institute of Astronomical Optics & Technology, Chinese Academy of Sciences, Nanjing 210008, China

Received 2019 September 2; accepted 2019 November 15

**Abstract** Site-testing is crucial for achieving the goal of scientific research and analysis of meteorological and optical observing conditions, one of the associated basic tasks. As one of three potential sites to host the 12-meter Large Optical/infrared Telescope (LOT), the Muztagh-ata site, which is located on the Pamir Plateau in Xinjiang, in west China, began its site-testing task in the spring of 2017. In this paper, we firstly start with an introduction to the site and then present a statistical analysis of the ground-level meteorological properties such as air temperature, barometric pressure, relative humidity, and wind speed and direction, recorded by an automatic weather station with standard meteorological sensors for a two-year duration. We also show the monitoring results of sky brightness during this period.

**Key words:** site-testing — meteorological condition — optical observing

### 1 INTRODUCTION

The international astronomical community has sustained great effort to find the best sites for the operation of large optical telescopes over the last few decades. An excellent site is a crucial condition for constructing such observational facilities, which determines its performance. In recent years, the projects spearheading new-generation astronomical facilities such as the Thirty Meter Telescope (TMT) (Schöck et al. 2009) and the Extremely Large Telescope (ELT) (Radu et al. 2012) have been committed to a comprehensive program of site selection and promoting the related site evaluation.

With the rapid growth of astronomy in China in recent years, an ambitious project, the Large Optical/infrared Telescope (LOT), with the goal to construct a 12-meter telescope, was selected to be built in the next decade. In order to maximize the performance of the telescope, a site

assessment campaign has been initiated for more than two years to identify the most suitable location to host it (Feng et al. 2020).

In the first decade of this century, Yao (2005) surveyed the astronomical resources in west China and suggested that the best candidate sites may be located in the eastern Pamirs. Through satellite photographs and a field survey of the Pamir Plateau, the Muztagh-ata site was identified as one of the three alternatives, with the other two being the Shiquanhe site in Tibet (Liu et al. 2020) and Daocheng site in Sichuan Province (Song et al. 2020). The gathering of meteorological data is essential prior to any investment in equipment or telescopes. The meteorological properties should be considered in site selection including air temperature, relative humidity, wind speed, wind gusts, etc. (Muñoz-Tuñón 2002; Jabiri et al. 2000; Tian et al. 2016). The best observing sites should have small daytime and nighttime air temperature gradients, high stability of the



**Fig. 1** The red pentagram in this map represents the location of the Muztagh-ata site. Its geographical location is  $38^{\circ}19'47''\text{N}$ ,  $74^{\circ}53'48''\text{E}$ , in the southwest of Xinjiang Uygur Autonomous Region of China.

air temperature during the night, small relative humidity, and low wind speed and wind gusts (Varela et al. 2014; Mahoney et al. 1998; Murdin 1985). Although the monitoring data are only available for two years and cannot provide conclusions on the climate in this area, statistical analysis of meteorological properties is available for the LOT campaign. Long-term analysis of the amounts of clouds through satellite data, data processing methods and results of all-sky images for this area were conducted in Cao et al. (2020a,b), during the period from 2017 March 10 to 2019 March 10; “clear” (No clouds) and “outer” (No clouds within the inner circle while some clouds are within the outer circle of all-sky images) account for 61.6% of nighttime and 63.1% of nights “clear” + “outer,” for more than three hours respectively.

The layout of this paper is as follows: In Section 2, we describe the Muztagh-ata site from the perspective of topography, traffic, surrounding social situation, etc. In Section 3, we detail the monitoring instruments. In Section 4, we provide the statistical results of site monitoring during the two years, which include air temperature, relative humidity, barometric pressure, wind speed and direction and sky brightness. In Section 5, we summarize the final conclusions.

## 2 SITE DESCRIPTION

The Muztagh-ata site is located in the eastern part of the Pamir Plateau, in the southwest of Xinjiang Uygur Autonomous Region of China. The geographical coordinates are  $38^{\circ}19'47''\text{N}$ ,  $74^{\circ}53'48''\text{E}$ , with an altitude of 4526 meters above sea level. The site location is given in the map<sup>1</sup> in Figure 1. Muztagh-ata, 7549 meters high, lies to the east of it, so we refer to our site as the Muztagh-ata site.

Our site lies to the southwest of the city of Kashgar, which is the third largest city in Xinjiang and has multiple good transport links. The site can be accessed by a 200 km national road from Kashgar. There are several high mountains taller than 5000 meters surrounding the site within a range of 100 km, blocking the Indian Ocean wet airflow and dust from the Tarim Basin from going to the site, which provide relatively stable weather conditions for this area. The local climate manifests characteristics of a typical plateau continental climate with an oxygen deficit which is cold, dry and receives little precipitation. According to the statistics provided by the local meteorological department, the local meteorological conditions are described as

<sup>1</sup> <https://map.baidu.com/>

follows: “The oxygen deficit is 30% ~ 40%. The annual average temperature is  $-6^{\circ}\text{C}$ . The most extreme low temperature recorded is  $-36^{\circ}\text{C}$ . The average annual precipitation is 271.1 mm and solid precipitation predominates, mostly in the late spring and summer. Southwest wind is the prevailing wind direction at the surface level.” These data indicate the existence of potentially good sites in this area for optical observations.

The light pollution situation is very good. Our site is in a sparsely populated region where herdsmen live for a very short time in summer. A national road passes by the foot of the mountain but the relative altitude between it and the site is  $\sim 900\text{ m}$ .

In Figure 2, a contour map<sup>2</sup> illustrates the topographic conditions surrounding the Muztagh-ata site, and there is a piece of a  $\sim 1\text{ km}^2$  flat region on the top of the mountain that can be available for accommodating the infrastructure required for a large telescope. The yellow pentagram in Figure 2 signifies the location of our monitoring point at present. So far, we have built two towers for the differential image motion monitor (DIMM) and some concrete foundations for various monitoring facilities there. Figure 3 displays a general view of the Muztagh-ata site.

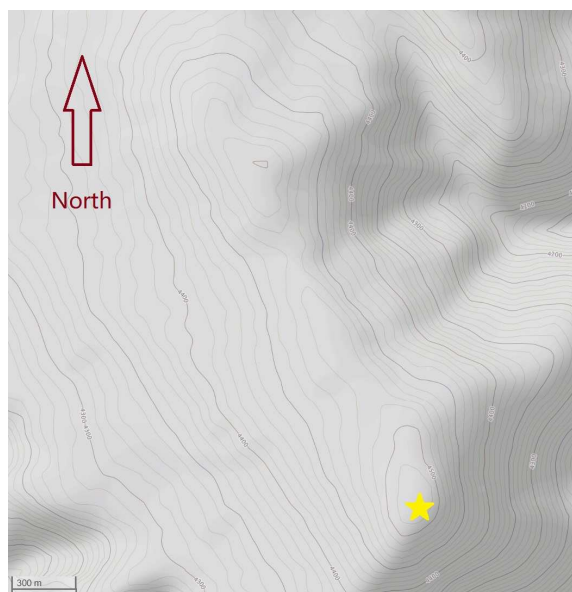


**Fig. 2** Contour map of the region surrounding our site. The yellow pentagram represents the location of our monitoring equipments at present.

### 3 MONITORING INSTRUMENTS – AUTOMATIC WEATHER STATION

Climatic parameters of our site are derived from the data supplied by an automatic weather station, which is a

<sup>2</sup> <https://www.openstreetmap.org/#=13/38.3473/74.9173&layers=C>

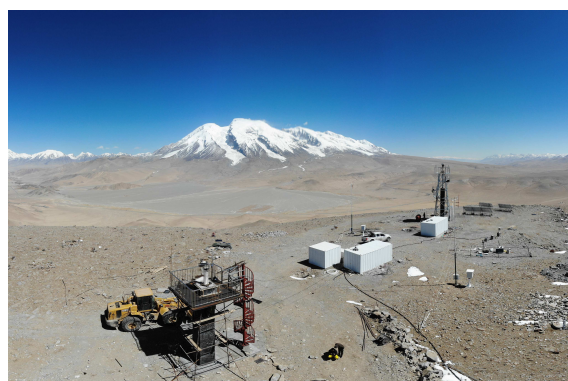


**Fig. 3** General view of the Muztagh-ata site. The snow-capped mountain that lies in the background is Muztagh-ata.

five-element commercial high-precision meteorological station. It measures and records air temperature, barometric pressure, relative humidity, wind speed and wind direction values. The anemometer and wind vane were supported by a 10-meter tower. The air-temperature sensor, hygrometer and barometer were set in a thermometer screen 1.5 meters from ground level. All of those sensors were calibrated to the specified absolute measurement accuracies in Table 1. The equipment was powered by solar panels and transmitted data through the GSM signal to a server hosted at National Astronomical Observatories, Chinese Academy of Sciences (NAOC) every 10 minutes, and the sampling interval was one minute.

The automatic weather station was installed on 2017 March 2. Several days of data records were absent in the two-year site testing because the GSM signal disappeared, caused by a power failure in the communication base stations. In addition, due to sensor failures, the recorded periods of each parameter vary, as shown in Table 1, last column.

## 4 SITE MONITORING RESULTS

### 4.1 Air Temperature

We analyze the differences in all meteorological parameters between the day and night. For this purpose, we define the time from the beginning of astronomical morning twilight to the end of astronomical evening twilight as daytime, and the rest of this day as nighttime. Figure 4 plots the daytime and nighttime air temperature with time at Muztagh-ata for the whole dataset during the measurement period indicated in Table 1. A strong seasonal dependency can be ascertained from this figure. The distributions and cumulative statistics for daytime and nighttime are displayed in Figure 5. The mean value of the daytime data is  $-1.9^{\circ}\text{C}$  and the median value is  $-1.0^{\circ}\text{C}$ . The mean value of the nighttime data is  $-6.9^{\circ}\text{C}$ , and the median value is  $-6.2^{\circ}\text{C}$ . There are two peaks in each histogram in

**Table 1** Range Accuracies and Recorded Periods of Meteorological Sensors

Element	Range	Accuracy	Recorded period
Air temperature ( $^{\circ}\text{C}$ )	$-50 \sim 50$	$\pm 0.1$	2017 Mar. 2~2019 Feb. 28
Relative humidity (RH%)	$0 \sim 100$	$\pm 3$	2017 Aug. 1~2019 Jul. 31
Wind speed ( $\text{m s}^{-1}$ )	$0.5 \sim 50$	$\pm 0.5$	2017 Mar. 2~2019 Feb. 28
Wind direction ( $^{\circ}$ )	$0 \sim 360$	$\pm 6$	2017 Mar. 12~2019 Feb. 28
Barometric pressure (hPa)	$300 \sim 1100$	$\pm 1$	2017 Mar. 2~2019 Feb. 28

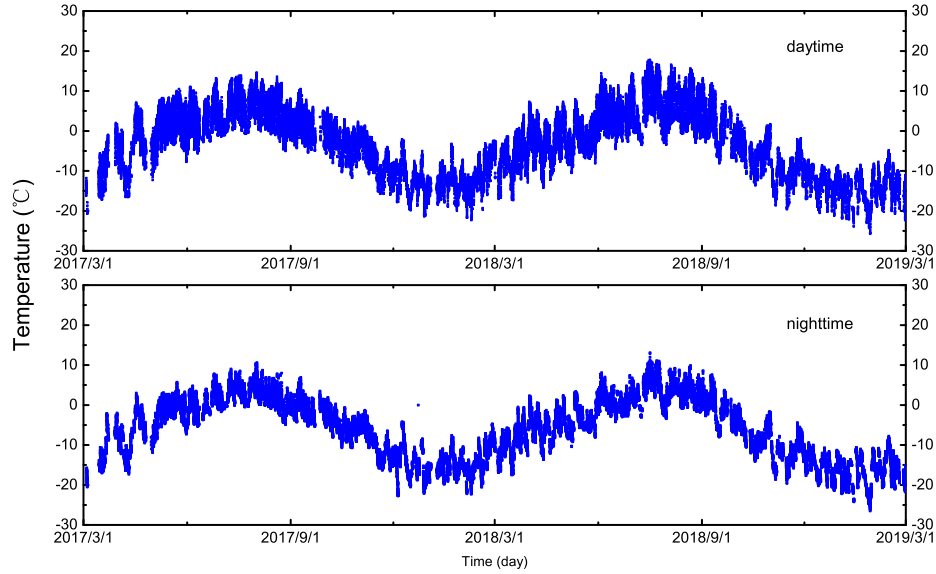
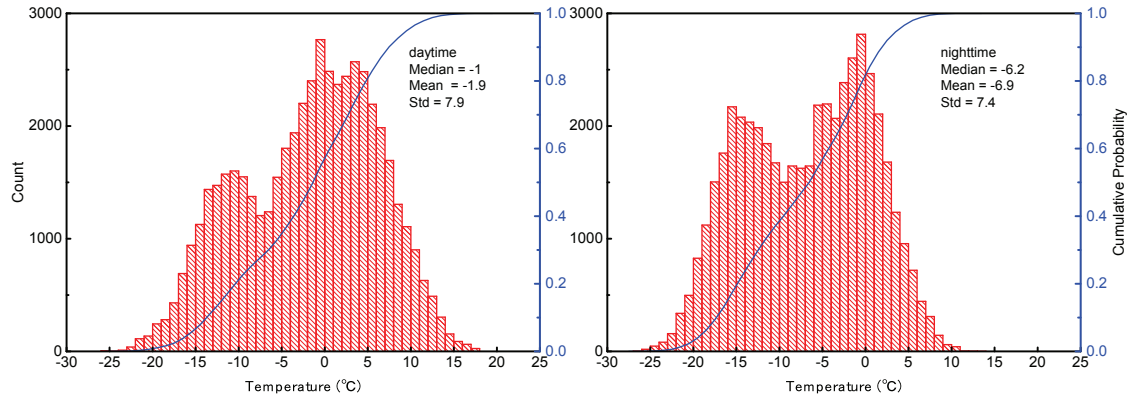
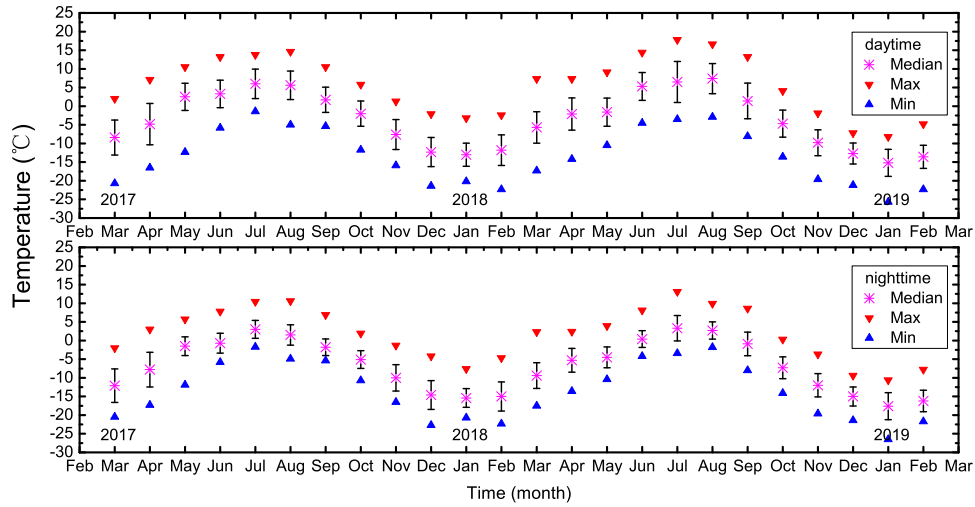
**Fig. 4** Air temperature values with time during daytime (*top*) and nighttime (*bottom*).**Fig. 5** Histograms and cumulative distributions of air temperature during daytime (*left*) and nighttime (*right*).

Figure 5, representing the median temperature values in summer and winter respectively.

We calculate the median, maximum and minimum values of the temperature per month from March 2017 to February 2019 during daytime and nighttime, separately as depicted in Figure 6. Error bars correspond to the standard deviation of the mean values. Detailed monthly statistical results are expressed in Table 2. January is the coldest month in this area with a daytime mean value of

$-14.1^{\circ}\text{C}$  and nighttime mean value of  $-16.4^{\circ}\text{C}$  while June is the warmest month with a daytime mean value of  $6.3^{\circ}\text{C}$  and nighttime mean value of  $3.2^{\circ}\text{C}$ . The maximum value ( $17.9^{\circ}\text{C}$ ) occurred on 2018 July 16 and the minimum value ( $-26.5^{\circ}\text{C}$ ) happened on 2019 January 28.

In order to explore the dependency of temperature differences during daytime and nighttime on season, we calculate the daily median and standard deviation values of the temperature differences during daytime and nighttime.



**Fig. 6** Monthly statistics of the air temperature during daytime (*top*) and nighttime (*bottom*) from March 2017 to February 2019.

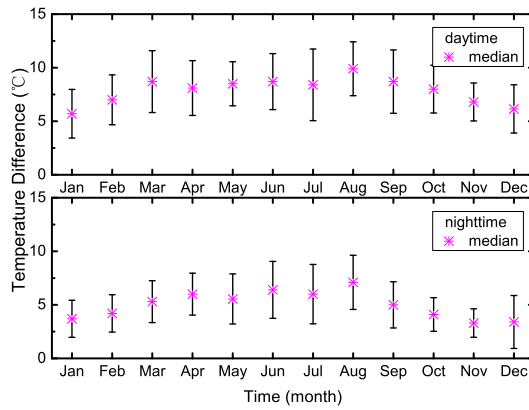


**Fig. 7** Monthly median and standard deviation values of temperature difference during daytime (*top*) and nighttime (*bottom*).

Then we display the monthly statistics in Figure 7. The median temperature differences are higher in warm seasons than in cool seasons. The median value of daily daytime temperature difference in August is  $9.9^{\circ}\text{C}$  and that at nighttime is  $7.1^{\circ}\text{C}$ .

#### 4.2 Relative Humidity

Because of sensor failure, relative humidity data are available only from August 2017 to July 2019, 24 months in total. Figure 4.2 shows the daytime and nighttime relative humidity with time during this period. The relative humidity and dew point are two important parameters for the astronomical instrumentation, because they control the occurrence of moisture and water condensation on the coldest parts of astronomical instrumentation, which determines whether the observation can be made (Lombardi et al. 2009). If the humidity is high enough, or when the dew

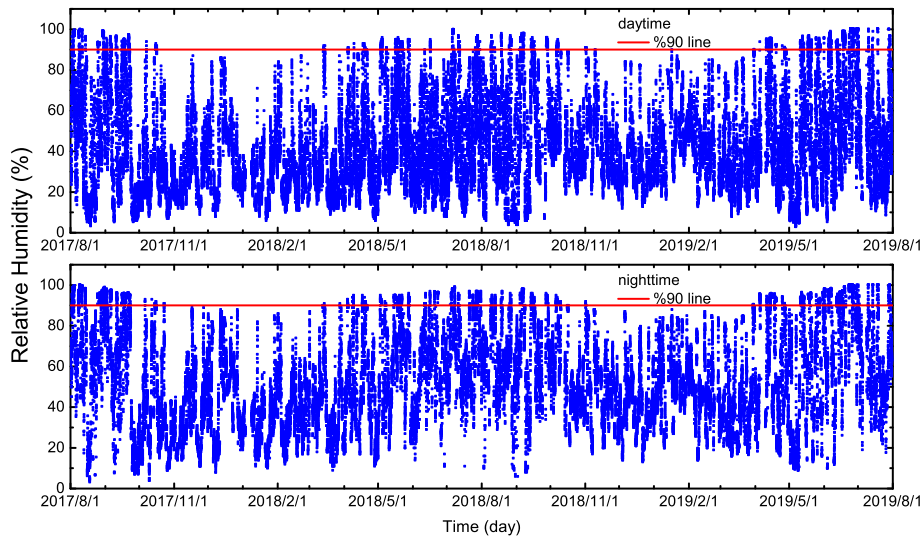
point temperature is very close to the air temperature, condensation will easily occur (Murdin 1985). Red lines in Figure 4.2 mark the 90% values representing the threshold, beyond which observations should be stopped. There are 6876 of the 95 817 data points which have values higher than 90%, accounting for 7.2%. The rate is 8.8% of nighttime data.

The distributions and cumulative statistics for relative humidity during daytime and nighttime are represented in Figure 9. The median value of daytime is 39% and it is 49% for nighttime. Monthly statistics during daytime and nighttime are depicted in Figure 10, and some detailed information on monthly statistics is provided in Table 3. The highest monthly average of nighttime data is 68.7% in June. The relative humidity is higher in late summer and autumn of each year.

It is important to know the percentage of observational time in which condensation may occur. For this purpose,

**Table 2** Monthly Statistics on Daytime and Nighttime Air Temperature Data

Month	Nighttime Temperature					Daytime Temperature				
	Max	Min	Median	Mean	Std	Max	Min	Median	Mean	Std
Jan.	-7.6	-26.5	-16.0	-16.4	3.4	-3.2	-25.7	-13.7	-14.1	3.7
Feb.	-4.7	-22.3	-15.6	-15.0	3.6	-2.4	-22.3	-12.7	-12.3	3.8
Mar.	2.3	-20.5	-10.3	-10.4	3.9	7.3	-20.7	-5.9	-7.0	4.5
Apr.	3.0	-17.3	-6.4	-6.7	4.1	7.3	-16.5	-3.1	-3.5	5.1
May.	5.7	-11.9	-1.7	-1.5	2.5	10.5	-12.3	2.0	2.5	3.6
Jun.	8.1	-5.8	-0.2	0.0	2.6	14.4	-5.8	4.0	3.9	3.8
Jul.	13.1	-3.4	3.1	3.2	3.0	17.8	-3.5	6.2	6.3	4.8
Aug.	10.6	-4.9	2.1	2.2	2.6	16.6	-5.0	6.4	6.2	4.0
Sep.	8.6	-8.0	-1.3	-1.3	2.8	13.2	-8.1	1.6	1.7	4.2
Oct.	1.9	-14.1	-5.9	-6.1	2.9	5.8	-13.6	-3.1	-3.3	3.7
Nov.	-1.3	-19.6	-11.2	-11.0	3.5	1.3	-19.6	-8.8	-8.6	4.0
Dec.	-4.2	-22.7	-14.9	-14.8	3.3	-2.1	-21.4	-12.5	-12.5	3.4
Total	13.1	-26.5	-6.2	-6.9	7.4	17.8	-25.7	-1.0	-1.9	7.9

**Fig. 8** Relative humidity with time during daytime (*top*) and nighttime (*bottom*) from August 2017 to July 2019 and 90% lines.**Table 3** Monthly Statistics on Daytime and Nighttime Relative Humidity Data

Month	Nighttime Relative Humidity					Daytime Relative Humidity				
	Max	Min	Median	Mean	Std	Max	Min	Median	Mean	Std
Jan.	88	10	43	44.7	17.9	90	6	39	39.9	19.0
Feb.	87	12	43	43.2	15.7	87	10	36	37.9	17.1
Mar.	91	9	39	43.3	19.2	92	8	31	36.6	20.0
Apr.	96	11	50	55.0	23.0	96	6	39	43.7	22.3
May.	97	9	62	58.6	26.0	97	3	43	47.3	26.1
Jun.	100	10	69	68.7	22.9	100	5	46	50.4	26.6
Jul.	100	11	63	66.2	19.5	100	8	45	47.5	23.2
Aug.	100	3	66	64.7	22.2	100	3	46	46.3	26.8
Sep.	98	6	68	63.7	26.8	98	4	50	51.0	29.5
Oct.	95	4	42	46.1	22.8	95	7	35	38.5	20.7
Nov.	92	11	43	43.2	18.1	91	9	35	38.6	18.6
Dec.	88	8	41	44.0	18.5	86	8	33	38.0	18.1
Total	100	3	49	52.2	23.2	100	3	39	43.6	23.7

we calculate the dew point temperature during nighttime by a theoretical model (Tovmassian et al. 2016), and list the statistics for every month from August 2017 to July 2019 in Figure 11. Usually, the instrumentation is a few degrees

lower than the air temperature, so we set  $3^{\circ}\text{C}$  as the upper limit for the difference between air temperature and dew point temperature. In Figure 11, the red line represents the lower limit of  $3^{\circ}\text{C}$ . Each box signifies the values in the

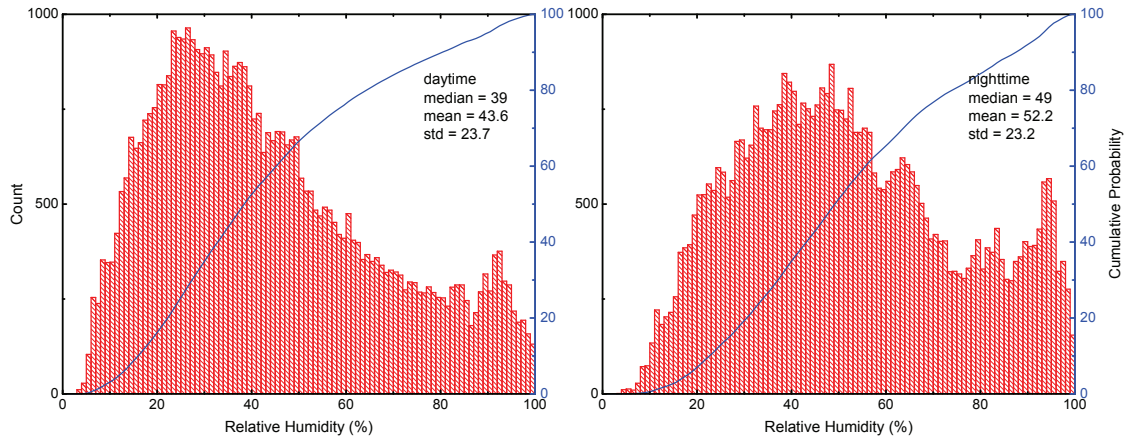


Fig. 9 Relative humidity histograms and cumulative distributions during daytime (left) and nighttime (right).

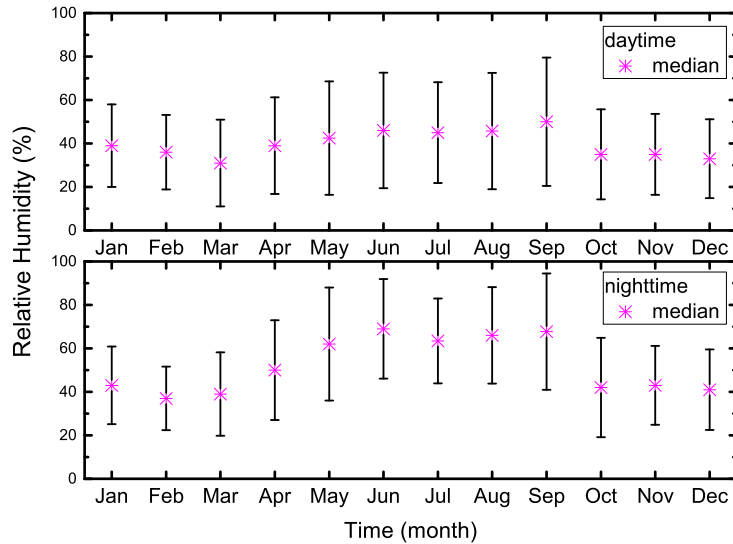


Fig. 10 Monthly median and standard deviation values of relative humidity during daytime (top) and nighttime (bottom).

range of 25% to 75% and the vertical lines mark the values 1% to 99%, and the diamonds and horizontal lines inside every box signify the mean and median values respectively. From Figure 11, we can see that the median values of differences between temperature and dew point temperature in autumn are closer to the red line than in other seasons, which indicates that condensation may occur frequently during autumn nights.

### 4.3 Barometric Pressure

Figure 12 displays the maximum, minimum, median and standard deviation values of air pressure data every month from March 2017 to February 2019. A clear positive correlation with air temperature can be observed in Figure 12. This indicates obvious plateau continental climate charac-

teristics which is higher and with a smaller variation range in warm seasons than in cool seasons.

The monthly maximum, minimum, median, mean and standard deviation values for daytime and nighttime are summarized in Table 4. The lowest air pressure (568.1 hPa) during the first year (March 2017 to February 2018) was exhibited in January 2018, whereas the highest air pressure (594.9 hPa) appeared in May 2017. The lowest (569.5 hPa) and highest (595.1 hPa) air pressures during the second year (March 2018 to February 2019) were recorded in February 2019 and October 2018 respectively. Statistics on daytime and nighttime data are displayed in Figure 13. The median value during daytime is 587.6 hPa and the mean value is 586.4 hPa. The median value during nighttime is 587 hPa and the mean value is 585.8 hPa. The air pressure is slightly lower during nighttime.

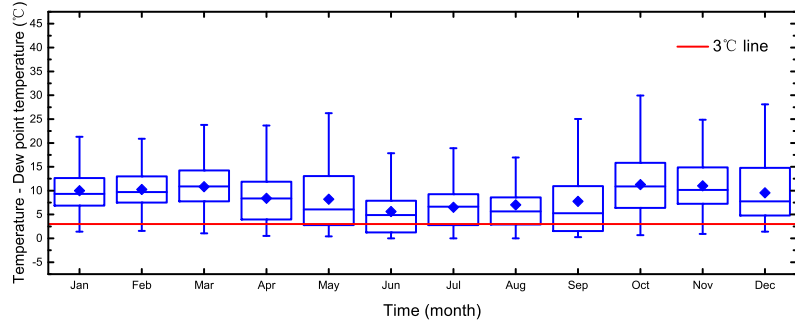


**Fig. 11** Boxplot of differences every month between temperature and dew point temperature during nighttime from August 2017 to July 2019. Each box represents the values in the range of 25% to 75% and vertical lines mark the values 1% to 99%. Diamonds and horizontal lines inside every box signify the mean and median values respectively. The red line corresponds to the upper limit of 3°.

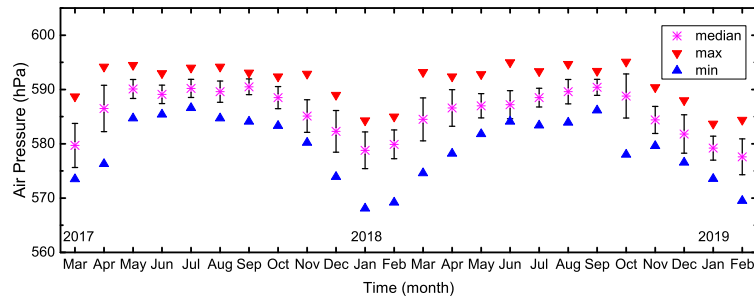


**Fig. 12** Monthly statistics on air pressure from March 2017 to February 2019.

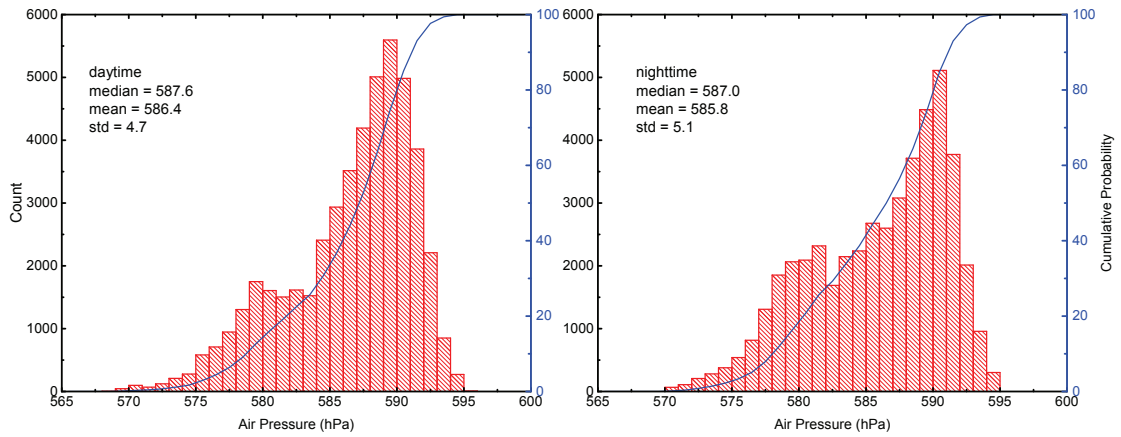


**Fig. 13** Air pressure histograms and cumulative distributions for daytime (*left*) and nighttime (*right*).

We analyze the air pressure in order to see if the site is dominated by high pressure which would imply prevailing stable good weather (Radu et al. 2012). The theoretically expected air pressure can be calculated by Equation (1) (US Standard Atmosphere model (Tovmassian et al. 2016)), where  $P_0 = 1013.25$  hPa is the sea level standard atmospheric pressure and  $T_0 = 288.15$  K (15° C) is the sea level standard temperature;  $h$  represents the altitude (4526 m) of our site.

$$P = P_0 \cdot \left(1 - 0.0065 \cdot \frac{h}{T_0}\right)^{3/5}. \quad (1)$$

When the air pressure is lower than the theoretically expected value, unstable weather may occur. We have computed the theoretically expected values for each time point during nighttime and compare them with the actual values to find out the frequency of unstable weather conditions monthly. The result is displayed in Figure 14. The percentage values in most of the months are roughly equal to 0%,

but obviously increase in spring from January to March. Especially in February, 17.8% of the nighttime period is dominated by low pressure.

#### 4.4 Wind Speed and Direction

Strong winds or gusts represent a serious hazard for the instruments (Tovmassian et al. 2016). Figure 15 shows the distributions and cumulative statistics for the wind speed during daytime and nighttime. The median values are  $6.5 \text{ m s}^{-1}$  and  $5.5 \text{ m s}^{-1}$  for daytime and nighttime respectively. Considering  $15 \text{ m s}^{-1}$  as the limit beyond which the telescope should be turned off and brought to the parking position, the percentage beyond this limit during nighttime is 6.6%.

Both high relative humidity values mentioned in Section 4.2 and strong wind constrain a telescope's operation, so it is essential to estimate their combined action. We calculated the percentage that either relative humidity is higher than the threshold of 90% or wind speed is stronger than  $15 \text{ m s}^{-1}$  during nighttime periods, and the result is 13%, which is roughly equal to the sum of 6.8% caused by high relative humidity and 6.6% caused by strong wind. It reflects the relative independence between high relative humidity and strong wind. Normally, high relative humidity comes with precipitation and clouds but strong wind may occur in a clear night, so strong wind has to be taken into account in addition to the amount of clouds when evaluating the annual observable time.

The daily trend of wind speed is plotted in Figure 16 where hourly medians and means are computed after merging different days. A clear time dependency can be ascertained such that the wind speed usually starts to increase at noon and reaches the peak before nightfall, then decreases gradually during the night. Relatively low wind speed in nighttime is beneficial to astronomical observation.

Monthly statistics for the nighttime measurements of wind speed are shown in Figure 17, in which each box represents values in the range of 25% to 75% and vertical lines mark the values 1% to 99%. Diamonds and horizontal lines inside every box signify the mean and median values respectively. The red line in Figure 17 corresponds to the upper limit of  $15 \text{ m s}^{-1}$ . It can be noticed that the wind speed is higher in cold seasons, and especially in these three months from January to March, the median of nighttime wind speed is higher than  $7 \text{ m s}^{-1}$ . This corresponds to the frequency of low barometric pressure as visible in Figure 14. More detailed statistics on wind speed during daytime and nighttime can be seen in Table 5.

The strength and direction of ground winds define the airflow conditions which influence the ground-layer turbulence (Geissler & Masciadri 2006). A wind rose diagram is one that gives the percentage of the time in which

the wind blows from each direction. It also indicates the strength of the wind velocity in the prevailing wind directions. Figure 18 shows the wind rose in daytime and nighttime during the period from 2017 July 12 to 2018 February 28, from which we can clearly see that the prevailing wind direction is from southwest at all times of the year. Stable wind direction means stable airflow conditions, which will provide good conditions for astronomical observations. It also indicates that the wind direction is influenced little by local topography.

#### 4.5 Sky Brightness

Our site was equipped with a commercial device, a Sky Background Meter (SBM), developed by the Unihedron Company for sky brightness monitoring from 2017 May 24 to 2018 February 28. The full width at half maximum (FWHM) of the angular sensitivity is about  $20^\circ$  in the zenith direction and the SBM data are sampled every minute. The histogram in the top panel of Figure 19 displays the distribution and cumulative statistics of the night sky brightness. The median value during nighttime is  $21.35 \text{ mag arcsec}^{-2}$  and 43.4% of the values are concentrated between  $21.5$  and  $22.3 \text{ mag arcsec}^{-2}$ . To remove the influence of moonlight, we show the sky brightness distribution during nighttime without the Moon (nighttime with the Moon height below  $-6^\circ$ ) in the bottom panel of Figure 19. The median value is  $21.74 \text{ mag arcsec}^{-2}$ .

## 5 SUMMARY AND CONCLUSIONS

A site evaluation has been initiated for identifying the best location in China to host the LOT project, and the Muztagh-ata site is one of the three candidates. We have studied the astro-climate conditions of the Muztagh-ata site based on the statistical analysis of parameters which directly effect astronomical observation, including air temperature, relative humidity, dew point temperature, barometric pressure, wind speed, wind direction and sky brightness, and highlighted the results in this paper.

We are aware of that two years of meteorological monitoring cannot be sufficient for a full site characterization, but the main results are as follows:

1. The mean value of nighttime air temperature is  $-6.2^\circ \text{ C}$  while it is  $-1.0^\circ \text{ C}$  for daytime. The maximum and minimum values during the two-year site-testing period are  $17.8^\circ \text{ C}$  and  $-26.5^\circ \text{ C}$  respectively. Temperature difference exhibits strong seasonal dependency, greater in warm seasons and smaller in cold seasons. The annual average temperature of the two years is  $-2.4^\circ \text{ C}$  (March 2017 to February 2018) and  $-5.1^\circ \text{ C}$  (March 2018 to February 2019) respectively. Compared with the result of  $-6^\circ \text{ C}$  provided by the local meteorological department, 2017 was

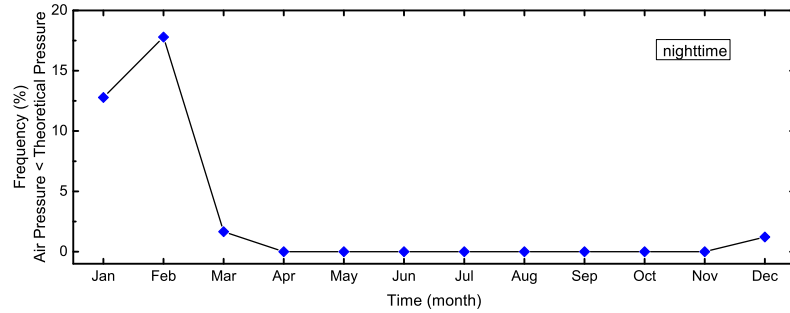


**Fig. 14** Monthly distributions of percentages for differences between air pressure and theoretical pressure whose values are less than 0 hPa during nighttime.

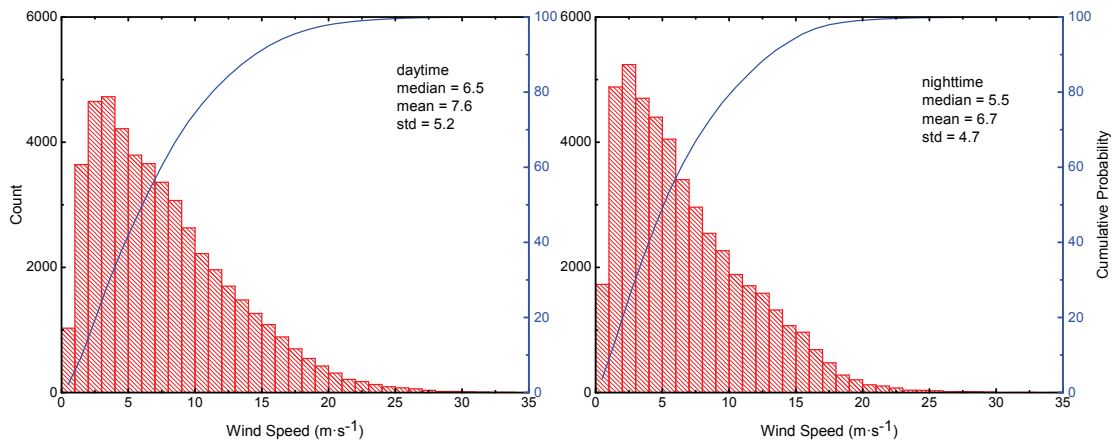


**Fig. 15** Wind speed histograms and cumulative distributions for daytime (*left*) and nighttime (*right*).

**Table 4** Monthly Statistics on Daytime and Nighttime Air Pressure Data

Month	Nighttime Air Pressure					Daytime Air Pressure				
	Max	Min	Median	Mean	Std	Max	Min	Median	Mean	Std
Jan.	586.5	570.1	579.4	578.6	2.9	584.3	568.1	579.1	578.9	2.8
Feb.	584.9	570.1	579.0	578.5	3.0	585.0	569.2	579.1	578.1	3.2
Mar.	593.1	574.4	583.8	583.6	3.9	593.2	573.5	583.8	583.8	4.3
Apr.	593.3	576.4	586.8	585.9	3.7	594.2	576.3	586.5	586.3	3.8
May.	594.6	582.9	590.0	588.9	2.3	594.5	581.8	589.3	589.4	2.5
Jun.	594.4	585.3	589.1	588.6	2.2	595.0	584.1	589.3	589.4	2.3
Jul.	594.1	584.7	589.8	589.3	1.8	594.0	583.4	589.3	589.9	2.0
Aug.	594.9	585.4	590.1	589.6	1.9	594.7	583.9	589.6	590.2	2.1
Sep.	593.7	583.9	590.7	590.3	1.4	593.4	584.1	590.4	590.7	1.5
Oct.	592.1	578.0	588.9	588.2	2.8	595.1	574.0	588.6	588.6	3.2
Nov.	589.2	580.1	584.8	585.3	2.7	592.9	579.6	584.8	585.2	2.8
Dec.	589.2	574.3	582.1	582.3	3.3	589.0	573.9	582.0	582.3	3.4
Total	594.9	570.1	587.0	585.8	5.1	595.1	568.1	587.6	586.4	4.7

significantly warmer, and more precipitation may have occurred in 2017 than during normal years. This is meaningful for analyzing the difference in the amount of clouds between these two years.

2. The median of relative humidity data for nighttime from August 2017 to July 2019 is 49% and it is 39% for daytime. The percentage of nighttime in which the relative humidity values are higher than 90% is 8.8% and under these conditions the telescope should be stopped. We found

that 59% of nighttime data are concentrated in the range from 20% to 60%. This is mainly due to the surrounding glaciers which play a certain role in stabilizing the relative humidity during the night.

3. In order to evaluate the risk of condensation, we have computed the monthly percentages for the difference values between dew point temperature and air temperature smaller than 3°C during night. The monthly median values are closer to 3°C in late summer and autumn than oth-

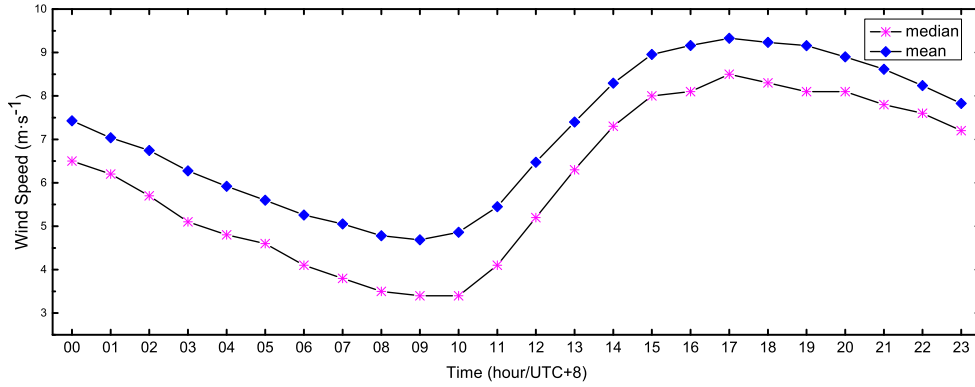


**Fig. 16** Mean and median values of hourly wind speed.

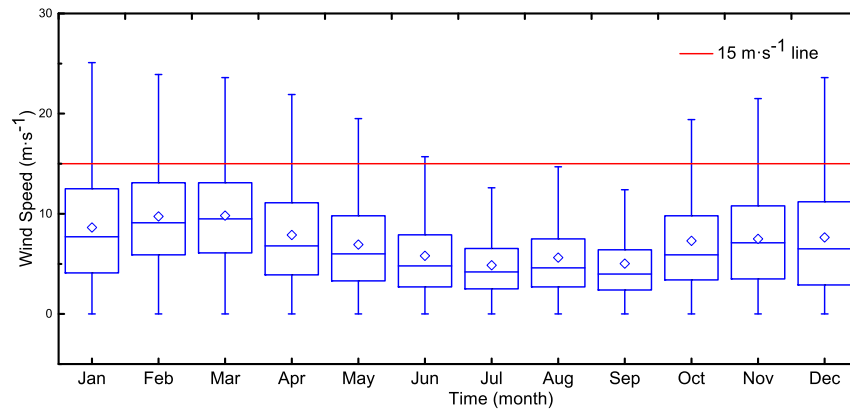


**Fig. 17** Boxplot of monthly wind speed during nighttime. Each box represents values in the range of 25% to 75% and vertical lines mark the values 1% to 99%. The diamonds and horizontal lines inside every box signify mean and median values respectively. The red line represents the upper limit of  $15 \text{ m s}^{-1}$ .

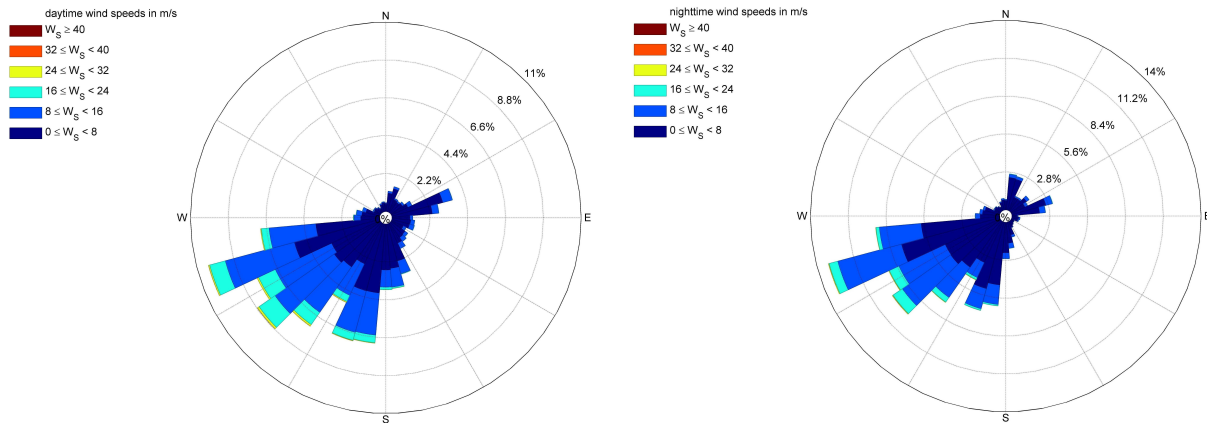


**Fig. 18** Wind rose density during daytime (left) and nighttime (right).

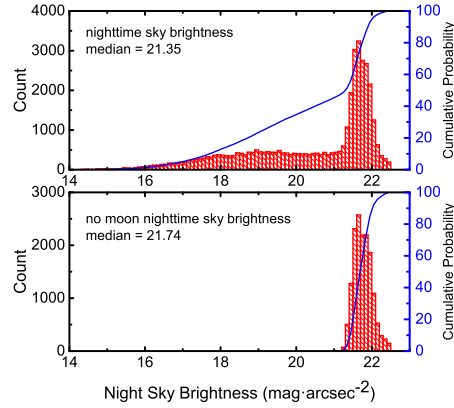


**Fig. 19** Distribution and cumulative statistics of the night sky brightness (*top*) and moonless nighttime (*bottom*).

**Table 5** Monthly Statistics on Daytime and Nighttime Wind Speed Data

Month	Nighttime Wind Speed				Daytime Wind Speed			
	Max	Median	Mean	Std	Max	Median	Mean	Std
Jan.	29.0	7.4	8.3	5.4	32.8	8.0	9.1	5.7
Feb.	29.3	8.6	9.0	4.6	35.3	10.2	10.6	5.8
Mar.	23.7	8.5	8.8	4.4	29.4	10.6	10.9	5.3
Apr.	27.8	6.0	7.2	4.8	30.9	7.5	8.4	5.2
May.	22.5	5.6	6.6	4.3	25.7	6.3	7.2	4.5
Jun.	20.7	3.9	4.8	3.5	30.6	5.5	6.4	4.3
Jul.	16.3	4.0	4.5	2.8	23.3	4.3	5.1	3.4
Aug.	21.4	4.3	4.8	3.2	25.5	5.0	6.2	4.4
Sep.	32.9	3.7	4.5	3.9	27.1	4.2	5.5	4.2
Oct.	34.9	5.0	6.5	5.0	36.6	6.9	8.2	5.6
Nov.	19.8	6.3	6.9	4.4	24.0	8.1	8.3	4.7
Dec.	33.2	5.8	7.1	5.3	37.1	7.6	8.6	6.0
Total	34.9	5.5	6.7	4.7	37.1	6.5	7.6	5.2

er seasons, which is mainly related to more precipitation in these months every year at the Muztagh-ata site.

4. Analysis of the barometric pressure data indicates typical plateau continental climate characteristics, lower and with a wider range in cool seasons. A pronounced seasonal dependence was represented in the monthly frequency of nighttime in which the air pressure value is lower than the theoretically expected value, which means unstable weather conditions are caused by it. The percentages are much higher in spring months, especially in February, during which it reaches 17.8%, than other months in which the rate roughly equals 0%.

5. The median value of nighttime wind speed is  $5.5 \text{ m s}^{-1}$  and it is  $6.5 \text{ m s}^{-1}$  for daytime. For 6.6% of the nighttime, the wind speed is greater than  $15 \text{ m s}^{-1}$ . We consider the wind speed distribution per hour and it can be clearly observed that the wind velocity usually increases in daytime and decreases in nighttime, which is good for nighttime observation. A strong correlation between wind speed distribution and low air pressure frequency was ascertained. The months whose frequencies of low air pres-

sure are relatively high have more occurrence of strong wind.

6. The prevailing wind directions are derived from the wind rose plot. The wind mostly comes from southwest during both daytime and nighttime, which could provide stable ground layer turbulence.

7. The median value of the sky brightness at the Muztagh-ata site measurements is  $21.35 \text{ mag arcsec}^{-2}$  and  $21.74 \text{ mag arcsec}^{-2}$  for no moon during nighttime. Through the analysis of images from an all sky camera, we found that the light pollution, mainly due to the lighting for the debugging of monitoring equipment during nights and the village or road surrounding our site, has little influence on the results.

**Acknowledgements** This work is supported by the National Natural Science Foundation of China (Grant Nos. 11873081 and 11603065) and the Operation, Maintenance and Upgrading Fund for Astronomical Telescopes and Facility Instruments, budgeted from the Ministry of Finance of China and administered by the Chinese Academy of Sciences.

**References**

- Cao, Z. H., Liu, L. Y., Zhao, Y. H., et al. 2020, *RAA (Research in Astronomy and Astrophysics)*, 20, 81
- Cao, Z. H., Hao, J. X., Feng, L., et al. 2020, *RAA (Research in Astronomy and Astrophysics)*, 20, 82
- Feng, L., Hao, J. X., Cao, Z. H., et al. 2020, *RAA (Research in Astronomy and Astrophysics)*, 20, 80
- Geissler, K., & Masciadri, E. 2006, *PASP*, 118, 1048
- Jabiri, A., Benkhaldoun, Z., Vernin, J., & Muñoz-Tuñón, C. 2000, *A&AS*, 147, 271
- Liu, L. Y., Yao, Y. Q., Yin, J., et al. 2020, *RAA (Research in Astronomy and Astrophysics)*, 20, 84
- Lombardi, G., Zitelli, V., & Ortolani, S. 2009, *MNRAS*, 399, 783
- Mahoney, T., Muñoz-Tuñón, C., & Varela, A. M. 1998, *New Astron. Rev.*, 42, 417
- Muñoz-Tuñón, C. 2002, in *ASPC Series*, 266, *The Astroclimatic Station: A Must for Any Major Observatory (Invited Speaker)*, eds. J. Vernin, Z. Benkhaldoun, & C. Muñoz-Tuñón, 498
- Murdin, P. 1985, *Vistas in Astronomy*, 28, 449
- Radu, A. A., Angelescu, T., Curtef, V., et al. 2012, *MNRAS*, 422, 2262
- Schöck, M., Els, S., Riddle, R., et al. 2009, *PASP*, 121, 384
- Song, T. F., Liu, Y., Wang, J. X., et al. 2020, *RAA (Research in Astronomy and Astrophysics)*, 20, 85
- Tian, J. F., Deng, L. C., Zhang, X. B., et al. 2016, *PASP*, 128, 105003
- Tovmassian, G., Hernandez, M.-S., Ochoa, J. L., et al. 2016, *PASP*, 128, 035004
- Varela, A. M., Vázquez Ramió, H., Vernin, J., et al. 2014, *PASP*, 126, 412
- Yao, Y. 2005, *Journal of Korean Astronomical Society*, 38, 113